Hindawi
Geofluids
Volume 2021, Article ID 3243243, 14 pages
https://doi.org/10.1155/2021/3243243

Research Article

Investigation of the Mechanical and Permeability Evolution Effects of High-Temperature Granite Exposed to a Rapid Cooling Shock with Liquid Nitrogen

Tianzuo Wang[1,2] **Linxiang Wang**[1] **Fei Xue**[1,2] **Mengya Xue**[1] **Hangcheng Xie**[1] **and Ningbo Tang**[1]

[1]*Key Laboratory of Rock Mechanics and Geohazards of Zhejiang Province, College of Civil Engineering, Shaoxing University, Shaoxing, Zhejiang 312000, China*
[2]*Zhejiang Collaborative Innovation Center for Prevention and Control of Mountain Geologic Hazards, Shaoxing, Zhejiang 312000, China*

Correspondence should be addressed to Fei Xue; xuefei@usx.edu.cn

Received 7 July 2021; Revised 12 September 2021; Accepted 25 September 2021; Published 25 October 2021

Academic Editor: José Luis Pastor

Liquid nitrogen (LN_2), which can greatly improve the efficiency of hot dry rock (HDR) mining, is commonly used as a cooling material in the enhanced geothermal system (EGS). Physical property, triaxial compression, and permeability tests were undertaken on treated granite samples, for a better scientific understanding of the effect of the LN_2 cooling method on the mechanical and permeability properties of the rocks after heat treatment. The experimental results indicated that the physical properties of the treated granite change significantly, such as the density and wave velocity are substantially reduced. Meanwhile, with the increase of treatment temperature, the macroscopic cracks on its surface are gradually generated and the volume is expanded clearly. In addition, the surface wettability of granite gradually increases with increasing temperature. Compared with the air/water cooling methods, under LN_2 cooling condition, the mechanical properties decrease markedly. When the temperature exceeds 600°C, the granite strength decreases significantly to only 56.16% of the reference value. The deformation properties also change significantly, with a final strain of about 3% at failure for a sample at 800°C, showing an obvious ductile deformation characteristic. Further, an appreciable correlation also exists between the initial permeability of granite and temperature. Once the temperature exceeds 200°C, the increase in temperature contributes to the increase in initial permeability. In addition to the effect of temperature, the increase in load also leads to a change in the permeability coefficient. When the temperature reaches 600°C, the permeability of granite first decreases and then increases with the increases in axial stress. The results of this paper are valuable in understanding the effect of thermal shock by LN_2 on the fracturing efficiency and permeability characteristics of dry hot rocks.

1. Introduction

Development of hot dry rock (HDR) resources plays an important role in meeting the demand for energy [1–5]. Generally, the geothermal energy is mainly stored in a hot granite reservoir, which is distributed at the depth of 2–6 km with a temperature above 150°C [6]. Due to the low permeability of reservoir matrices, the permeability enhancement technologies are often suggested to improve the thermodynamic efficiency and productivity of the enhanced geothermal system [7, 8]. Liquid nitrogen (LN_2) cryogenic fracturing has been proven to be an efficient stimulation method, which has a great potential in establishing pathways with high permeability [9, 10]. During the process of cryogenic fracturing, the use of LN_2 can produce a high thermal gradient and a rapid temperature change in the rock inner and outer body, leading to a greater thermal stress and more thermal cracks in HDRs compared with traditional water/air cooling [11]. Water was often used as a coolant in previous works, but water has the disadvantage that can even cause important reductions

in the mechanical properties of nonheat-treated rocks [12, 13]. Consequently, the physicomechanical properties of the HDR reservoirs are greatly influenced by LN_2 cooling treatments. The effects of different thermal shocks by water cooling on physical properties, mechanical behaviors, and permeability parameters of rocks are critical knowledge for the successful reformation of deep geothermal reservoirs [14].

In recent years, plentiful in-depth studies on the physical and mechanical properties of granites after high-temperature treatment have been conducted, and many valuable conclusions have been obtained by various investigators. Previous experimental studies have indicated that thermal-induced microcracks are formed in granite after high-temperature treatment, which was caused by thermal expansion and uneven temperature distribution of minerals [13, 14]. Once the critical temperature is reached, macroscopic cracks developed inside the rock by expansion of mineral particles further contributing to the high-temperature erosion of granite [15, 16]. Zhang et al. [17] analyzed in detail the effect of temperature variations on the distribution of several variables in the physical field and the cracking by an improved hydrothermal-salt-mechanical (IHTSM) model. Shao et al. [18, 19] found that rapid cooling would instigate more thermal cracking within the granite, leading to more pronounced deterioration of mechanical properties. Subsequently, they considered the potential causes of the thermal sensitivity discrepancy among the three rocks based on the result of scanning electron microscope (SEM) and X-ray diffraction (XRD) [8]. However, Wu et al. [20] indicated that the uniaxial compressive strength (UCS) of granites cooled in water did not drop a lot until the rock temperature reached to 400°C. At higher cooling rates, the strength and elasticity of the granite might be further reduced under strong thermal shock. Chen et al. [21] indicated that the peak stress of heated granite decreases with the heating temperature increases (from 200°C to 1,000°C). Brotóns et al. [22] found that the thermal stress produced by the temperature gradient can degrade physical properties of the stone as the temperature increases (from 105°C to 600°C). Liu and Xu [23] investigated physical and mechanical properties of granite and sandstone after high-temperature treatment (from 100°C to 1,000°C) and found that 400°C is the sensitivity point for strength.

Recently, researchers have shown an increased interest in the relationship between high-temperature treatment and permeability, because the permeability of granite may increase in thermal-induced microcrack formation and propagation. Chen et al. [24] carried out compression tests and found the change in permeability was negligible before microfracture coalescence, and when the crack was in the growth region, it increased dramatically. Subsequently, to understand the effect of temperature on the permeability properties of granite, Chen et al. [21, 25] found that the thermal sensitivity temperature of permeability is 500°C. Then, Tian et al. [26] found a significant effect on initial and residual permeabilities of granite with increases of 3-4 orders of magnitude under temperatures from 25°C to 750°C by air cooling.

However, in contrast to the study of the mechanical properties of rock, there is much less information about the effects of LN_2 cooling on permeability characteristics. Despite the importance of permeability for the extraction of HDR, there remains a paucity of evidence on the permeability evolution pattern of granites after high-temperature heating and LN_2 cooling treatment. Thus, the aim of this essay is to explore the effect of different heating temperatures on the mechanical and permeability properties of granite under the action of LN_2 cooling. The granite samples were subjected to heating-cooling in four levels, i.e., a slow heating to 200°C, 400°C, 600°C, and 800°C followed by a rapid cooling with LN_2. A comparative analysis was conducted to study the variations in the physicomechanical and permeability behavior of granite subjected to different heating-cooling thermal shocks.

2. Materials and Methods

2.1. Sample Preparation. Granite, as a typical rock type in HDR [17], was selected as experimental materials in our study. The granite specimens were collected from an outcrop located at Hunan Province, China. According to the mineralogical analyses using X-ray diffraction (XRD), the granite is primarily composed of feldspar (47.6%), quartz (15.7%), and biotite (23.8%). The rock samples were shaped into the standard cylinders of $\Phi 50 \times 100$ mm in the laboratory according to the International Society for Rock Mechanics (ISRM) standards [27]. Figure 1(a) shows the rock samples and test setup used in our experiment. The thermal loading schedule is shown in Figure 1(b). In the first step, 12 granite samples were divided into four groups, which were all first heated to different target temperatures (200°C, 400°C, 600°C, and 800°C) using a high-temperature furnace with a heating rate of 2°C/min and then were kept at the preset temperature for 2 h. Secondly, the heated specimens were taken out of the high-temperature furnace and placed in a tank with 25 L of liquid nitrogen. Finally, granite specimens with treatment completed were installed on the designated device, as shown on the right side of Figure 1(a).

2.2. Testing Methods

2.2.1. Physical Parameter Test Procedure. Prior to mechanical testing, the average and standard deviations of physical properties of the sample, such as density, size (i.e., height and diameter), and P-wave velocity, were first measured before heating and after cooling. The contact angle of droplets is an important indicator of rock wettability which reflects the hydrophilic properties of the rock, as shown in Figure 2(a). Wanniarachchi [28] provided the wettability test method which is using the high-definition image technique to obtain the contact angle of water droplets on the granite surface and the method schedule as follows. Firstly, the syringe was cleaned using distilled water and filled with water. Secondly, a clean surface specimen was placed stably on a horizontal table. Subsequently, a water droplet was slowly injected by the syringe on the surface of the granite, as shown in Figure 2(a). Finally, a high-definition camera was used to record interfacial surface tension around the droplet. The contact angle of the rock sample surface is the

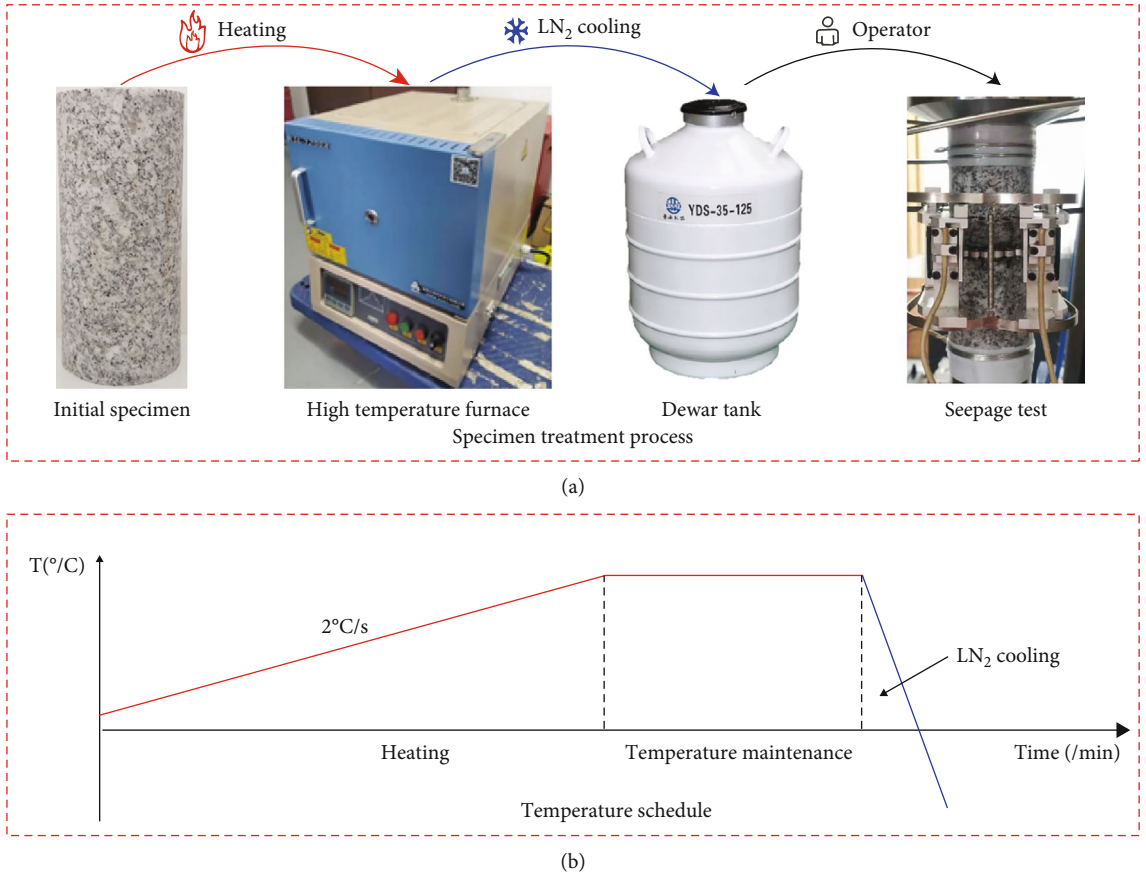

Figure 1: (a) Rock samples and experimental instruments. (b) Thermal shock process of granite.

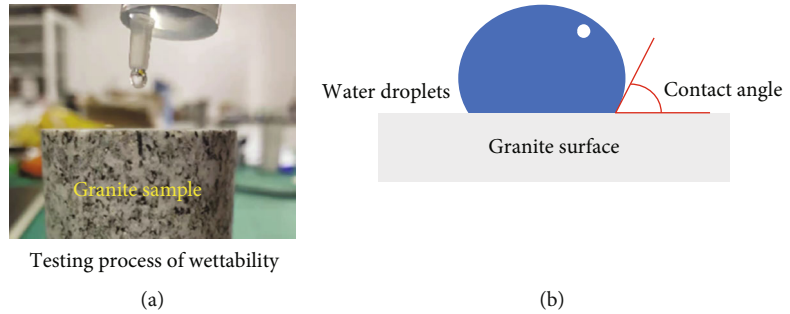

Figure 2: Testing process of granite wettability and contact angle diagram.

angle between the contour line of water droplet with the horizontal of rock surface, as shown in Figure 2(b).

2.2.2. Mechanical Test Procedure. Triaxial compression tests were performed using the MTS815.04 rock mechanics test system on the thermal shock-treated granite specimens, as shown in Figure 3. The system can perform triaxial deformation experiments at confining stress up to 140 MPa, axial load up to 4600 kN, and hydraulic pressure up to 140 MPa and can measure the permeability of rock samples down to 1×10^{-20} m^2. This study used deionized water as the pore fluid and silicone oil as the confining pressure fluid. The confining and inlet pressures were controlled by an oil pressure intensifier and a gas pressure pump, respectively. The triaxial compression strength was obtained with a confining pressure of 5 MPa, a confining pressure rate of 0.1 MPa/s, and an axial displacement loading rate of 0.001 mm/s.

2.2.3. Permeability Test Procedure. Considering that granite has ultralow permeability, the transient-pulse permeability test method was used to guarantee the measurement accuracy [29], as shown in Figure 4. To investigate the permeability evolution of thermal shock-treated samples with increasing deviatoric stress, the following test procedures were designed:

(i) The treated specimens were saturated in water for 48 h and then jacketed with 0.5 mm thick Teflon

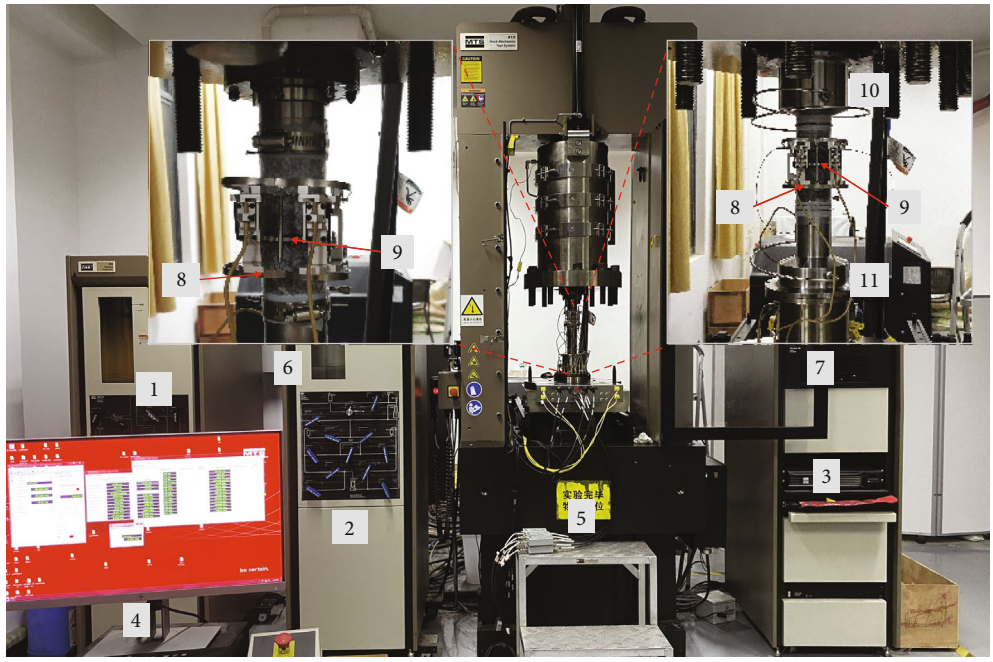

Figure 3: Rock mechanics test system (MTS815.04): (1) confining pressure intensifier, (2) pore pressure intensifier, (3) digital control, (4) computer control, (5) test loading of frame, (6) conventional triaxial device, (7) permeability testing device, (8) axial LVDT, (9) lateral LVDT, (10) upper loading plate, and (11) bottom loading plate.

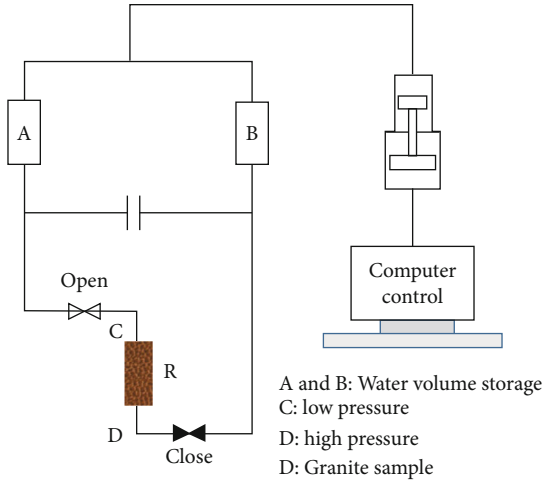

Figure 4: Illustration of the transient method.

heat shrink tubing, sealed at both ends with several stainless-steel wires

(ii) The assembled jacketed sample was then placed into a triaxial pressure cell with the hydrostatic pressure set at 5 MPa

(iii) The circumferential pressure was held at 5 MPa and the axial stress was increased by a displacement-controlled manner with a deformation rate of 0.001 mm/s

(iv) From this stage, the sample permeability was measured until the peak stress was reached. For each permeability test, 3 MPa of hydraulic pressure was applied at both the top and bottom ends

(v) The hydraulic pressure at the top surface was decreased to 1 MPa in order to create a pressure gradient between the two end surfaces. Water flowed from the bottom end of the sample to the top end and through the interior of the sample

It is important to note that this water pressure should be lower than the confining pressure to avoid lateral leakage.

The ΔP-t curves recorded were used to calculate the sample permeability values according to Equation (1). It was noted that the limiting load and axial load were kept constant while the permeability measurements were performed. The permeation test was terminated when the pressure gradient reached or approached 0.4 MPa, the permeation time reached 3 h, or the permeation pressure difference stabilized. In the permeability test measured by the transient method, the water pressure difference (ΔP) between the two ends of the specimen decreased gradually, and the rate of decrease depended on the rock type, rock configuration, specimen length, specimen cross-sectional area, water density and viscosity, and stress state [29].

$$k = \frac{c_f B H \mu}{2tA} \ln \frac{\Delta P_0}{\Delta P_f}, \tag{1}$$

where k is the permeability of the rock sample, c_f is the compressibility of the water, B is the volume of the upper and lower reservoirs, H is the length of the specimen, μ is the viscosity of the water, t is the duration of the test, A is

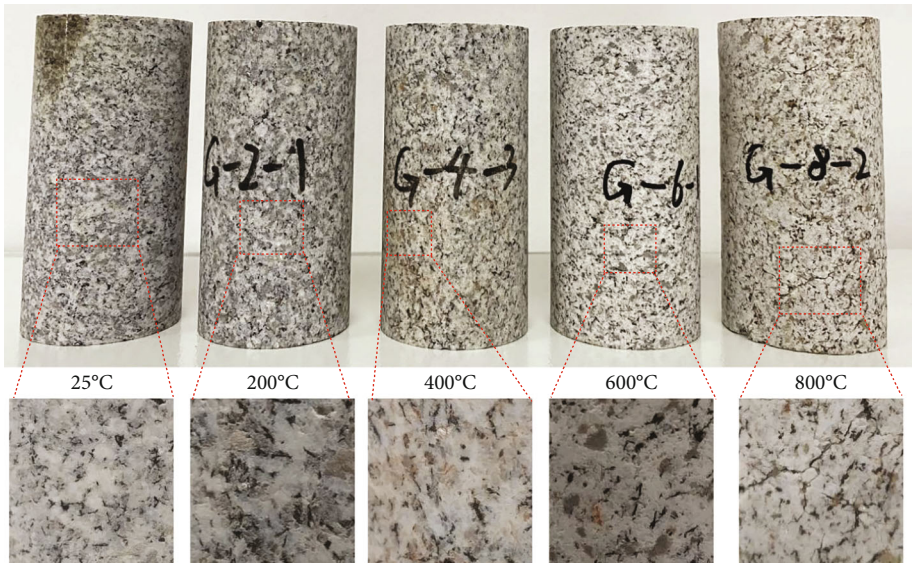

Figure 5: Surface morphology of granite specimens after different thermal shocks (25°C, 200°C, 400°C, 600°C, and 800°C).

the cross-sectional area of the specimen, and P_f is the difference in water pressure between the upper and lower ends of the rock specimen. Well-known parameter values are $c_f = 453 \times 10^{-12}$ Pa^{-1}, $B = 175$ cm^3, $H = 100$ mm, $\mu = 1 \times 10^{-3}$ Pa · s, $A = 19.625$ cm^2, $\Delta P_0 = 3.0$ MPa, and $\Delta P_f = 1$ MPa.

3. Results and Discussion

3.1. Physical Properties

3.1.1. Surface Morphology, Density, and P-Wave Velocity. The surface morphology graphs of granite samples subjected to different thermal shock treatments (200, 400, 600, and 800°C) are shown in Figure 5. According to previous investigations, the escape of adsorbed water, crystalline water, and tectonic water existed in the rocks during the high-temperature treatment [30]. The gravity and hydroscopic water escaped completely at about 150°C and 200°C, respectively [31]. As a result, as shown in Figure 5, there is no visible difference between the surface colors of granite samples at 25°C (with no thermal shock treatment) and those of granite samples at 200°C. With further increase in temperature, when at 600°C, the quartz experienced an α-β phase transition, which caused a significant fading of the surface color [32, 33].

The basic physical and mechanical properties of granite samples subjected to LN_2 cooling under different temperatures are summarized in Table 1. The relationships between P-wave velocity and density and temperature for granite samples heated to different temperatures followed by LN_2-coling treatment are depicted in Figure 6. It can be seen from Figure 6 that the variation in P-wave velocity exhibits a noteworthy downward trend with a relatively small initial reduction at 200°C and then an approximately linear rapid decrease with further rise of temperature. However, the density apparently does not change before 600° and is reduced by approximately 20% at 800°C. These results indicate that the P-wave velocity, compared with the density, is more sensitive and more suitable for characterizing the damage caused by thermal shock to granite.

3.1.2. Wettability. The results of wettability quantified by contact angle for different thermal shock-treated granite samples are shown in Figure 7. It can be found that the contact angles of the water droplet are increased with the heating temperature, and the angles are 63° at 25°C, 147° at 200°C, 165° at 400°C, 170° at 600°C, and 178° at 800°C (Figures 7(a)–7(f)). The results suggest that the thermal shock-treated granite surface is more hydrophilic than the untreated granite surface, and water is more readily absorbed on the treated granite surface. It is noteworthy that the surface of the granite after the 800°C treatment has obvious macroscopic cracks and a large number of fine cracks. This allowed the water droplets to be immediately absorbed into the interior as soon as they made contact with the rock surface. The water stains produced by water penetration can be seen in the top view, as shown in Figure 7(f).

3.2. Mechanical Behavior

3.2.1. Stress-Strain Curves. The triaxial compressive stress-strain curve of the granite sample with no thermal treatment at room temperature (25°C) under the confinement pressure of 5 MPa is illustrated in Figure 8. It can be seen that the curve can be divided into four stages, i.e., (i) compaction stage (O-A), (ii) elastic stage (A-B), (iii) yield stage (B-C), and (iv) failure stage (after the C point) [34]. The characteristic stresses corresponding to each stage in the triaxial compression curve are point A (crack closure stress), point B (damage threshold stress), and point C (peak stress). Each stress levels are selected for permeation tests to observe the permeation characteristics of granite under different stages,

Table 1: Average of physical and mechanical parameters of granite specimens under different thermal shock conditions.

	Heating temperature (°C)	Diameter (mm)	Height (mm)	Weight (g)	Density (kg/m^3)	P-wave velocity (m/s)	Strength (MPa)
Before	25	49.15	100.72	501.4	2.63	3472	/
After		49.15	100.72	501.4	2.63	3472	185.26
Before	200	49.24	99.97	501.2	2.63	3458	/
After		49.26	100.05	500.8	2.63	3226	166.75
Before	400	49.41	100.32	503.8	2.62	3442	/
After		49.41	100.34	503.3	2.62	2688	156.48
Before	600	49.35	99.76	509.3	2.67	3460	/
After		49.85	100.34	508.3	2.60	1621	151.86
Before	800	49.24	100.32	501.8	2.63	3481	/
After		51.42	103.92	500.8	2.32	823	80.29

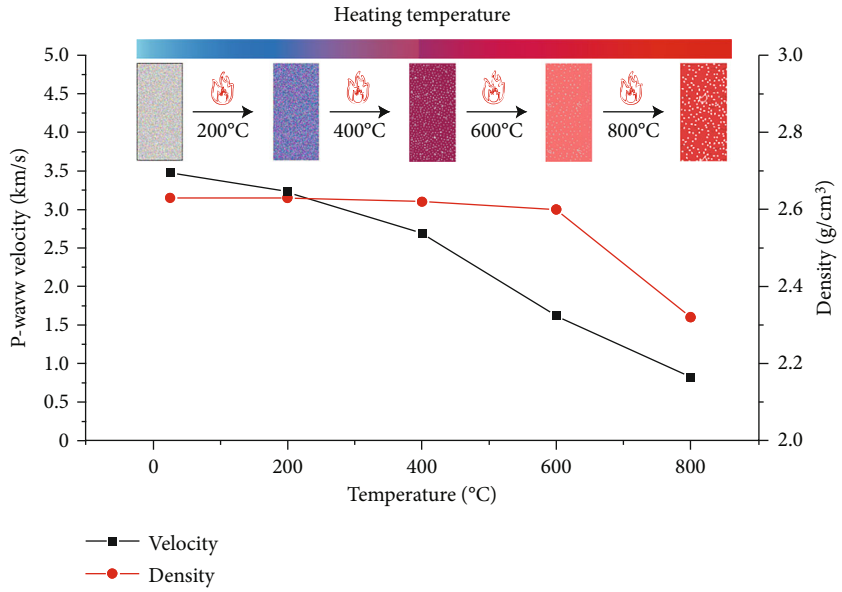

Figure 6: Density and P-wave velocity change with temperature of granite sample.

and the experimental results will be presented in the next section.

The stress-strain curves under hydronic-mechanical coupling condition of granite samples after exposure to different thermal shock treatments are plotted in Figure 9. It can be seen that the stress-strain responses of five specimens have obvious differences, suggesting that thermal shock has a significant effect on the mechanical behavior. With the increase in heating temperature, the initial nonlinear deformation segment induced by the closure of preexisting microcracks becomes more and more pronounced, especially if the temperature is over 600°C. Then, in the linear growth segment, as the temperature increases, the slope of the curve becomes lower and lower. Meanwhile, the decline of the curve in the postpeak segment gradually changes from a sudden drop to a slow drop, especially at 800°C, which shows a clear transformation from brittleness to ductility. These changes all can be attributed to more thermal cracks occurring in the sample led by the rapid release of thermal stress under the action of extreme temperature difference.

3.2.2. Triaxial Compressive Strength. The changes of the triaxial compressive strength of granite samples after heating and LN_2 cooling treatment under a confining pressure of 5 MPa are shown in Figure 10. It can be seen from Figure 10 that the triaxial compressive strength of granite does not change significantly during temperatures of 25~400°C. This phenomenon indicates that when the heating temperature is relatively low, only physical morphology variation and slight microcrack initiation occurred in granite with the escape of absorbed, bound, and crystalline water [14]. As the temperature increases, further and exceeding 573 degrees, more thermal-induced microcracking transferred into macrocracks as a result of the phase change of quartz [30]. Due to the formation of macrocracks, thermal stresses were released, and the continuous increase in temperature promoted the formation of more microcracks [33]. In particular, when the temperature reached 800°C, a large amount of crystal and structural water escaped, and Mg^{2+} oxidation in the black mica led to a large amount of thermal change, which eventually induced macroscopic

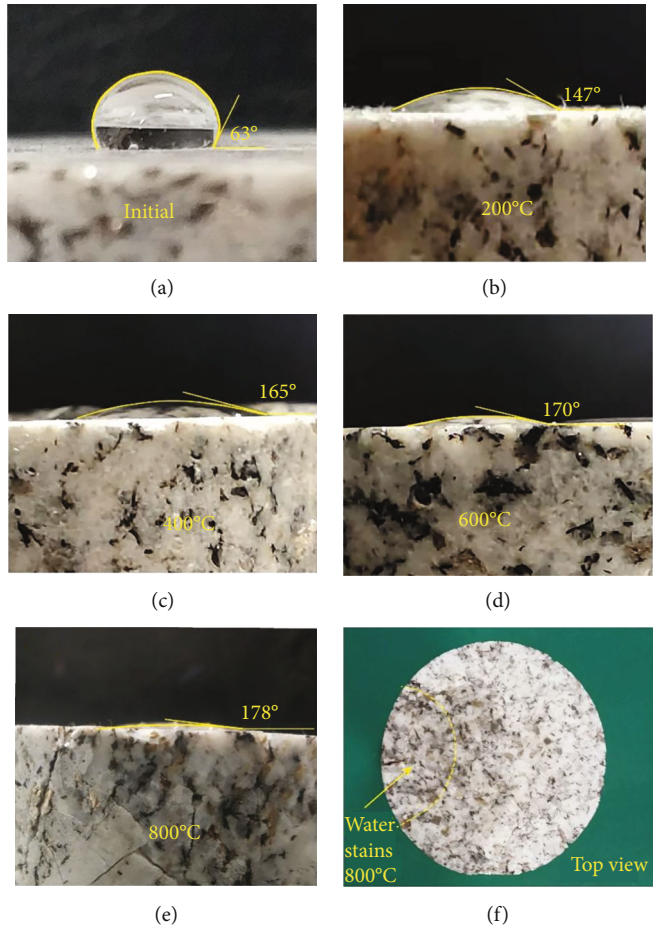

Figure 7: Contact angle images of granite samples after different thermal shock treatments.

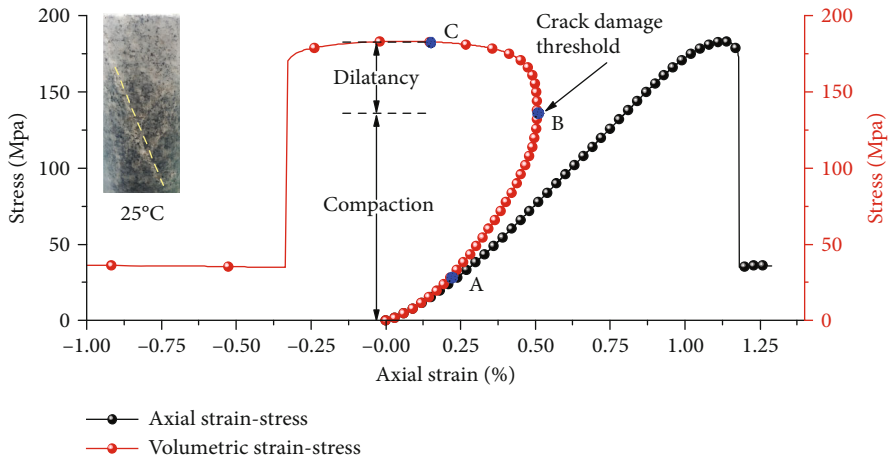

Figure 8: Stress-strain curves of granite sample at room temperature with no thermal shock treatment.

crack formation. Therefore, the peak strength remained relatively constant at the temperature of less than 600°C. When the temperature reached 600°C, some metal bonds (such as Al-O, K-O, Na-O, and Ca-O) broke, and some minerals (such as calcium carbonate and calcium montmorillonite) melted or decomposed [35]. More cracks were induced by heating, and the peak strength of granite decreased significantly at 800°C.

To further comparatively analyze the effect of the cooling method on the fracturing efficiency of dry hot rock, the relationships between triaxial compressive strength and temperature under air and water cooling conditions reported in

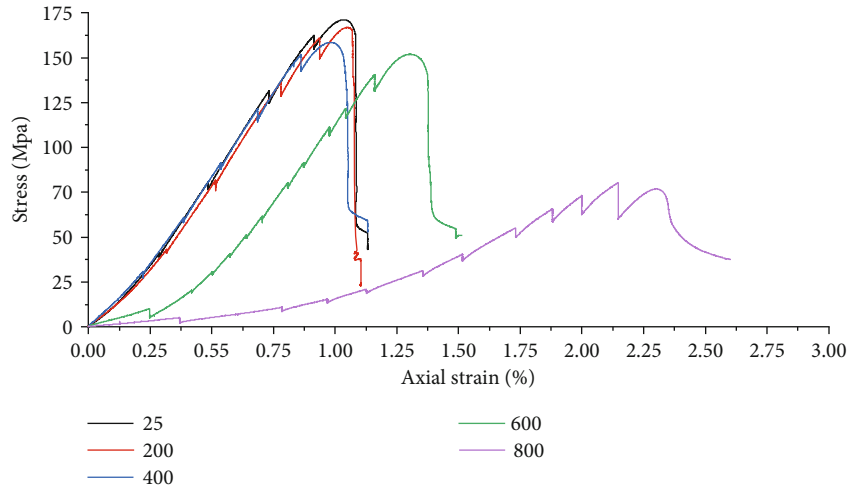

Figure 9: Stress-strain curves of granite samples after different thermal shock treatments.

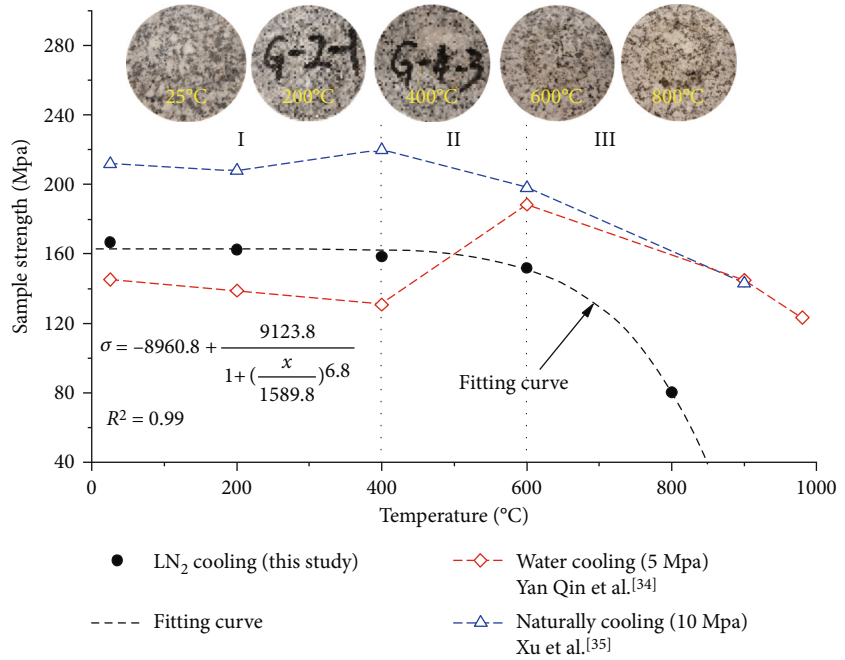

Figure 10: Triaxial compressive strength of granite samples after being subjected to different thermal shock treatments under confining pressure of 5 MPa.

previous studies are also plotted together in Figure 10. It can be found that the variation trend of granite strength with temperature can be divided into three stages, which are (I) 25°C-400°C, (II) 400°C-600°C, and (III) above 600°C. Under either air or water cooling condition, the granite strength shows a trend of fluctuation with the change of temperature [35, 36], and there is a critical temperature of transition from strengthening to weakening. Under the LN_2 cooling condition, however, the strength of granite showed a sustained decreasing trend with increasing temperature, which conformed to the quadratic function. When the temperature reached 800°C, the granite strength decreases significantly and reaches 80.29 MPa. These differences in results indicate that at a certain heating temperature range, the relatively low cooling rate is more likely to lead to the closure or healing of preexisting microcracks than to the expansion and initiation of cracks.

3.2.3. Failure Pattern. Final failure patterns of granite samples subjected to different thermal shock treatments under triaxial compression are presented in Figure 11. When the temperature is at 25°C, the angle of the main macroscopic fracture with respect to the horizontal direction is about 60°, as shown in Figures 11(a) and 11(b). When the temperature rises to 200°C, 400°C, and 600°C, the angle of the macroscopic fracture is dominated by large-angle tensile fractures of 70°-80°, as shown in Figures 11(c)–11(e). The difference of macrocracks is owing to the temperature field

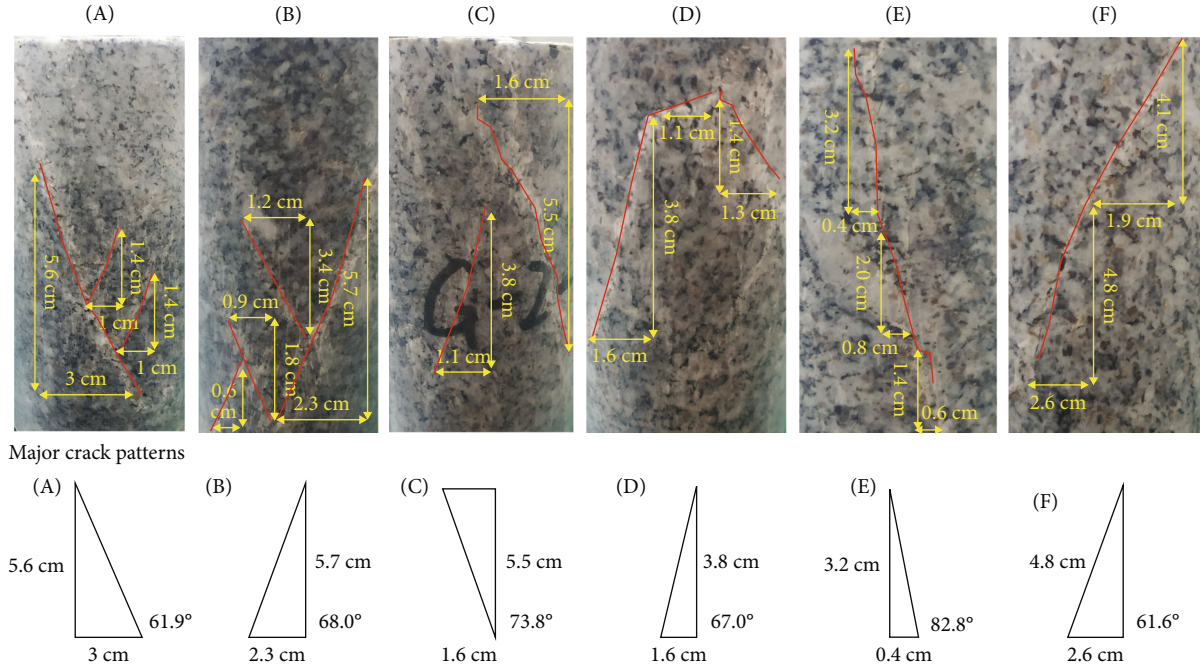

Figure 11: Failure patterns of granite samples subjected to different thermal shock treatment conditions: (a) 25°C, (b) 25°C, (c) 200°C, (d) 400°C, (e) 600°C, and (f) 800°C.

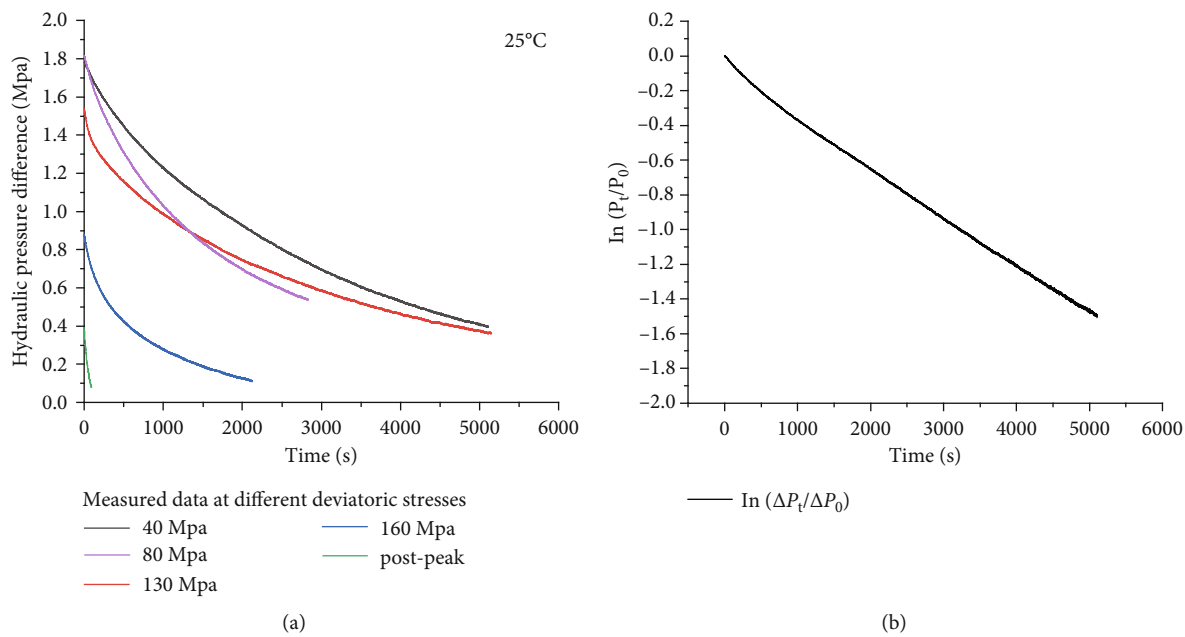

Figure 12: (a) Relationship between hydraulic pressure difference and time in four stages during triaxial compression and (b) linearization of differential pressure decay data of sample at 25°C under axial stress of 40 MPa.

heterogeneous distribution and the thermal stress in minerals (tensile) under rapid quenching. At failure, there are many large-angle macroscopic tensile fractures, which is due to the decrease of tensile resistance with the increase of temperature [37]. As a result, the granite transforms from brittle to ductile deformation.

3.3. Permeability Parameters. During the process of hydraulic-mechanical coupling loading, the pores and microcracks in the treated granite can produce some complex dynamic volume changes, resulting in the permeability evolution characteristics of granite. The time taken for the permeability pressure difference (ΔP) to reach stability and

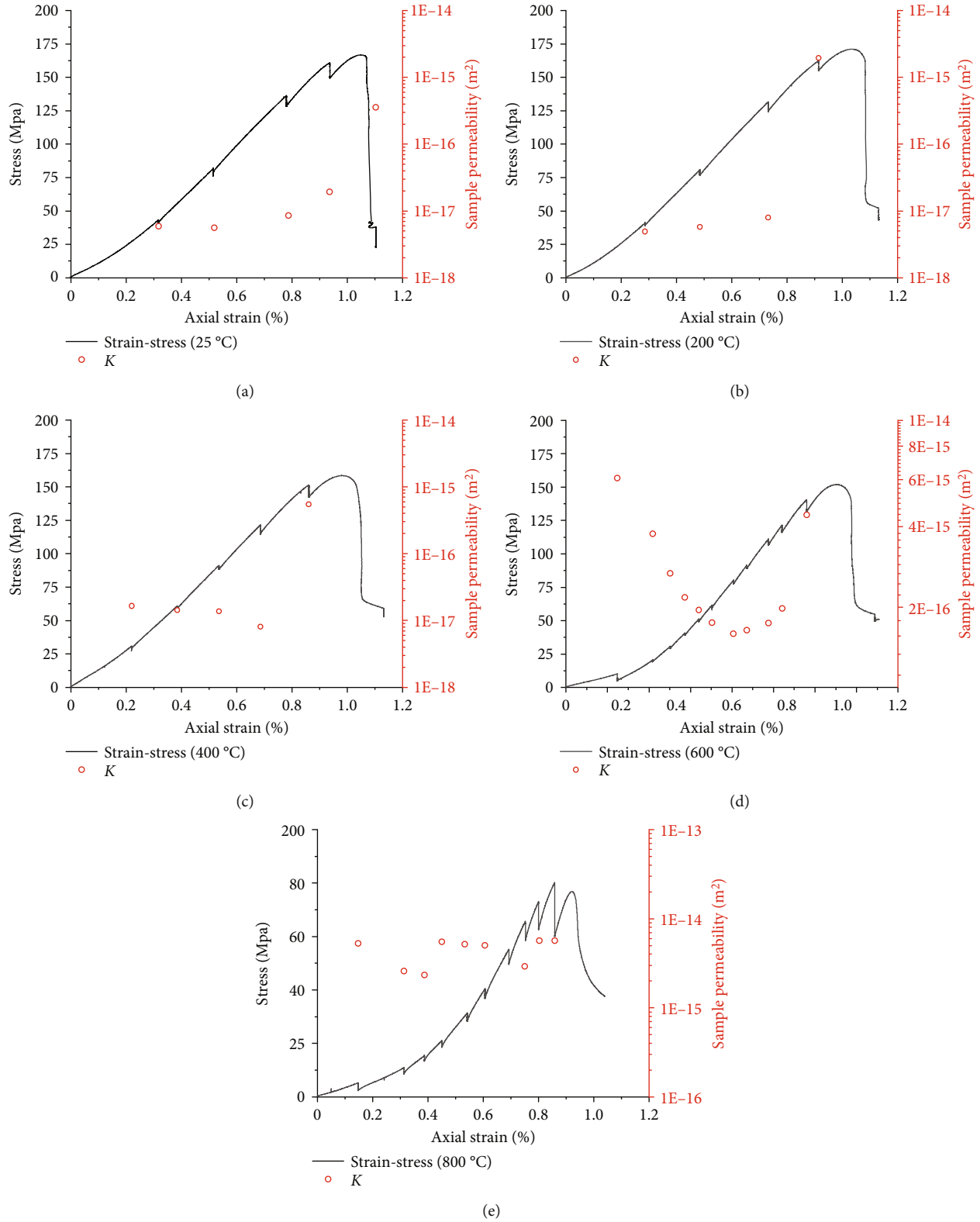

Figure 13: Evolution of deviatoric stress and sample permeability as a function of axial strain.

to decrease below 0.5 MPa at the same ΔP which is related to the stress state of the granite can be seen in Figure 12(a). In addition, it is noteworthy that with the time increase, the initial ΔP decreases gradually and cannot reach the preset 2 MPa as presented in Figure 12(a), because of the development of internal cracks in the granite with loading increase. In particular, at the yield stage, the initial ΔP is below to 0.5 MPa, as shown in Figure 12(a).

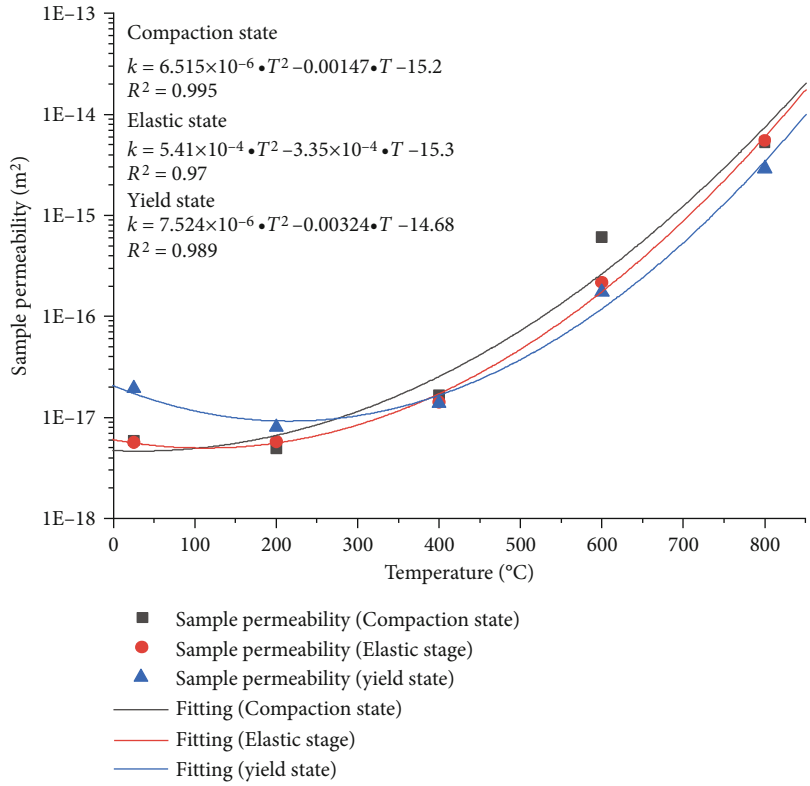

Figure 14: Relationship between permeability evolution and treatment temperature under different stress stages.

After the logarithm fetch on the $\Delta P/\Delta P_0$, the typical evolution law of the logarithm of permeability pressure with loading time under percolation is shown in Figure 12(b). The typical example of experimental data are linearly fitted to obtain slope $m_1 = -2.8 \times 10^{-4}$, fitted correlation coefficient $R^2 = 99.6\%$, $c_f = 453 \times 10^{-12}\ \text{Pa}^{-1}$, $B = 175\ \text{cm}^3$, $H = 100\ \text{mm}$, $\mu = 1 \times 10^{-3}\ \text{Pa}\cdot\text{s}$, and $A = 19.625\ \text{cm}^2$, which are finally calculated based on Equation (1): $k = 5.6 \times 10^{-4}\ \text{m}^2$.

To examine the permeability evolution during triaxial compression, the curves of deviatoric stress and sample permeability as a function of axial strain for each heating temperature are plotted in Figure 13. The granite samples under different thermal shock treatments exhibit a similar mechanical behavior: (1) A certain degree of stress recession occurs during each percolation, which is caused primarily by grain slipping during percolation. (2) In the process of percolation, the fluid under the action of ΔP passed through the crack channel which may cause further damage to rock and also reduce the stress.

As shown in Figures 13(a)–13(c), the permeability evolutions of granite samples at 200°C and 400°C are similar to the reference sample (25°C). Before reaching 0.8% of the axial strain, the permeability is relatively stable and floats around 1×10^{-17}. It is due to the fact that the crack channels are not fully formed during this stage. When the axial strain continues to increase and the axial stress approaches the peak value of stress, the permeability of the sample increases significantly by nearly two orders of magnitude to 1×10^{-15}, manifesting that liquid seepage channels have been fully developed inside the sample. In addition, the permeability of samples exhibits an interesting phenomenon at 600°C, as shown in Figure 13(d). The permeability decreased first and then increased with the increase of the axial strain, and the turning point of the axial strain is 0.8%. It is due to the closure of a large number of thermally induced cracks during the initial stage, leading to a decrease in permeability reaching 1.8×10^{-17}. Thereafter, the incremental generation of new cracks induced by compression results in the increase of permeability. Moreover, as exhibited in Figure 13(e), the permeability evolution pattern of the granite after being treated at 800°C shows a distinct difference with other temperature-treated samples. The permeability changes in all loading stages are relatively slight and always fluctuate around $1.6 \times 10^{-15}\ \text{mm}^2$, which is significantly larger than the permeability at low heating temperature. This can be contributed to a large number of macroscopic thermal damage cracks existing inside the granite, and the thermal-induced cracks are hard to close even during the action of compression.

To further analyze the effect of treatment temperature on permeability characteristics under different stages, typical permeability data (average values) were selected to obtain the correlation between permeability and temperature, as shown in Figure 14. It can be seen that the permeability of thermal-treated granite during the elastic stage is positively correlated with temperature. In addition, the permeability

coefficient in the elastic stage is lowest for each treated granite because of the initial crack closure caused by compression. Thereafter, with the increase of stress, the initiation and coalescence of microfissures and then transformation into macroscopic fractures provide a rapid flow passage for fluids.

Moreover, there is a significant quadratic relationship between temperature and permeability, as illustrated in Figure 14. In the compression-density stage, temperature is greatly affected the permeability of the sample. Permeability of the rock sample increased with the change of temperature in this stage. A similar characteristic has been exhibited in the elastic stage, which is weakly influenced by temperature at 200°C. During the yield stage, there is a phenomenon that the permeability variations show decrease at first and then increase with the increase of temperature. The permeability at the compression stage reached the minimum when the granite is exposed to temperatures between 200°C and 400°C. At the compression-density stage, the permeability is lowest when the rock was under thermal treatment. When the treatment temperature is below 400°C, flow channels can remain open and improve the permeability of the rock which is attributed to the loss of absorbed and bound water [38]. Furthermore, the loss of mineral water may damage the mineral skeleton, and this mineral damage will cause the rock to be denser and the brittleness of the rock increases, which leads to the additional improvements of permeability [39, 40]. When the temperature exceeds 400°C, the stress state takes effect on the compacting of the initial fracture, resulting in a decrease in permeability. When the treatment temperature is exactly 400°C, the change of permeability with the stress state is not obvious indicating that the 400°C is a turning point.

4. Conclusion

Rapid thermal shock can greatly improve the efficiency of HDR fracturing, especially with the use of LN_2. In this study, the influence of different thermal shocks (slow heating to different temperatures followed by rapid cooling with LN_2) on the physical, mechanical, and permeability properties of granite samples was systematically studied. Nondestructive tests (surface morphology, density, P-wave velocity, and wettability) and destructive tests (triaxial compression and seepage) were adopted to investigate these properties. Furthermore, based on the experimental results, a comparative analysis was conducted to study the variations in the physicomechanical and permeability behavior of granites after different thermal shock treatments. The main conclusions are summarized as follows.

(1) The LN_2, an efficient coolant, can change the physical properties of HDR by rapid cooling. Notably, the P-wave velocity of granite is reduced to nearly 80%, when the treatment temperature is at 800°C. Additionally, with the increase of temperature, a large number of thermal damage cracks are produced inside granite specimens, and the wettability of granite is enhanced. The fluid directly penetrates the granite interior and cannot form a complete water droplet under high-temperature treatment, which leads to the granite wettability being stronger, especially at 800°C treatments

(2) The effect of LN_2 cooling on the mechanical property of granite is significant. When the temperature exceeds 600°C, the strength of granite exhibits a distinct decrease, only 56.16% of the reference sample. Moreover, the deformation properties also change apparently; especially at 800°C, the final strain at the time of failure reaches about 3%, showing an obvious ductile deformation characteristic

(3) A correlation also exists between the initial permeability of granite and temperature. The permeability evolution pattern of granite after liquid nitrogen treatment shows a quadratic relationship with temperature. When the treatment temperature is lower than 400°C, the increase of stress enhances the impermeability of granite and makes the permeability coefficient decrease. When the temperature reaches 600°C, the permeability of granite first decreases and then increases with the increase of axial stress. With the temperature of treatment further increased, a large number of connected fractures are sprouted inside the rock, leading to an abnormally rapid seepage process and a larger calculated permeability coefficient

Data Availability

The data used to support the findings of this study are included in the article.

Conflicts of Interest

The authors declare that they have no conflicts of interest.

Acknowledgments

The authors would like to acknowledge the financial support for this study supported by the Second Tibetan Plateau Scientific Expedition and Research Program (grant No. 2019QZKK0904), the National Natural Science Foundation of China (grant Nos. 42007254 and 41831290), and the Natural Science Foundation of Zhejiang Province (grant No. LQ20E080006).

References

[1] C. Otto and T. Kempka, "Thermo-mechanical simulations confirm: temperature-dependent mudrock properties are nice to have in far-field environmental assessments of underground coal gasification," *Energy Procedia*, vol. 76, pp. 582–591, 2015.

[2] Y. J. Zhang, Z. W. Li, L. L. Guo, P. Gao, X. P. Jin, and T. F. Xu, "Electricity generation from enhanced geothermal systems by oilfield produced water circulating through reservoir stimulated by staged fracturing technology for horizontal wells: a case study in Xujiaweizi area in Daqing oilfield, China," *Energy*, vol. 78, pp. 788–805, 2014.

[3] A. K. Verma, P. Gautam, T. N. Singh, and R. K. Bajpai, "Discrete element modelling of conceptual deep geological repository for high-level nuclear waste disposal," *Arabian Journal of Geosciences*, vol. 8, no. 10, pp. 8027–8038, 2015.

[4] B. Chakrabarti, T. Yates, and A. Lewry, "Effect of fire damage on natural stonework in buildings," *Construction and Building Materials*, vol. 10, no. 7, pp. 539–544, 1996.

[5] M. Hajpál, "Changes in sandstones of historical monuments exposed to fire or high temperature," *Fire Technology*, vol. 38, no. 4, pp. 373–382, 2002.

[6] K. Breede, K. Dzebisashvili, X. Liu, and G. Falcone, "A systematic review of enhanced (or engineered) geothermal systems: past, present and future," *Geothermal Energy*, vol. 1, no. 1, 2013.

[7] D. L. Gallup, "Production engineering in geothermal technology: a review," *Geothermics*, vol. 38, no. 3, pp. 326–334, 2009.

[8] X. Wu, Z. Huang, S. Zhang et al., "Damage analysis of high-temperature rocks subjected to LN_2 thermal shock," *Rock Mechanics and Rock Engineering*, vol. 52, no. 8, pp. 2585–2603, 2019.

[9] S. R. Grundmann, G. D. Rodvelt, G. A. Dials, and R. E. Allen, "Cryogenic Nitrogen as a Hydraulic Fracturing Fluid in the Devonian Shale," in *SPE Eastern Regional Meeting*, Pittsburgh, Pennsylvania, 1998.

[10] R. Liu, H. Jing, X. Li, Q. Yin, Z. Xu, and M. He, "An experimental study on fractal pore size distribution and hydro-mechanical properties of granites after high temperature treatment," *Fractals*, vol. 29, no. 4, pp. 1–13, 2021.

[11] K. Kim, J. Kemeny, and M. Nickerson, "Effect of rapid thermal cooling on mechanical rock properties," *Rock Mechanics and Rock Engineering*, vol. 47, no. 6, pp. 2005–2019, 2014.

[12] R. Rabat, M. Tomás, T. M. Cano, and T. Miranda, "Impact of water on peak and residual shear strength parameters and triaxial deformability of high-porosity building calcarenite stones: interconnection with their physical and petrological characteristics," *Construction and Building Materials*, vol. 262, article 120789, 2020.

[13] M. Rabat, R. T. Cano, and R. Tomás, "Effect of water saturation on strength and deformability of building calcarenite stones: correlations with their physical properties," *Construction and Building Materials*, vol. 232, article 117259, 2020.

[14] V. Martínez-Ibáñez, M. E. Garrido, C. Hidalgo Signes, and R. Tomás, "Micro and macro-structural effects of high temperatures in Prada limestone: key factors for future fire-intervention protocols in Tres Ponts tunnel (Spain)," *Construction and Building Materials*, vol. 286, article 122960, 2021.

[15] F. E. Heuze, "High-temperature mechanical, physical and Thermal properties of granitic rocks– A review," *International Journal of Rock Mechanics and Mining Sciences*, vol. 20, no. 1, pp. 3–10, 1983.

[16] R. D. Dwivedi, R. K. Goel, V. V. R. Prasad, and A. Sinha, "Thermo-mechanical properties of Indian and other granites," *International Journal of Rock Mechanics and Mining Sciences*, vol. 45, no. 3, pp. 303–315, 2008.

[17] X. Zhang, E. Zhai, Y. Wu, D. Sun, and Y. Lu, "Theoretical and numerical analyses on hydro–thermal–salt–mechanical interaction of unsaturated salinized soil subjected to typical unidirectional freezing process," *International Journal of Geomechanics*, vol. 21, no. 7, pp. 1–11, 2021.

[18] S. Shao, P. L. P. Wasantha, P. G. Ranjith, and B. K. Chen, "Effect of cooling rate on the mechanical behavior of heated Strathbogie granite with different grain sizes," *International Journal of Rock Mechanics and Mining Sciences*, vol. 70, pp. 381–387, 2014.

[19] W. G. P. Kumari, P. G. Ranjith, M. S. A. Perera, B. K. Chen, and I. M. Abdulagatov, "Temperature-dependent mechanical behaviour of Australian Strathbogie granite with different cooling treatments," *Engineering Geology*, vol. 229, pp. 31–44, 2017.

[20] X. Wu, Z. Huang, H. Song et al., "Variations of physical and mechanical properties of heated granite after rapid cooling with liquid nitrogen," *Rock Mechanics and Rock Engineering*, vol. 52, no. 7, pp. 2123–2139, 2019.

[21] Y. L. Chen, J. Ni, W. Shao, and R. Azzam, "Experimental study on the influence of temperature on the mechanical properties of granite under uni-axial compression and fatigue loading," *International Journal of Rock Mechanics and Mining Sciences*, vol. 56, pp. 62–66, 2012.

[22] V. Brotóns, R. Tomás, S. Ivorra, and J. C. Alarcón, "Temperature influence on the physical and mechanical properties of a porous rock: San Julian's calcarenite," *Engineering Geology*, vol. 167, pp. 117–127, 2013.

[23] S. Liu and J. Xu, "Study on dynamic characteristics of marble under impact loading and high temperature," *International Journal of Rock Mechanics and Mining Sciences*, vol. 62, pp. 51–58, 2013.

[24] L. Chen, J. F. Liu, C. P. Wang, J. Liu, R. Su, and J. Wang, "Characterization of damage evolution in granite under compressive stress condition and its effect on permeability," *International Journal of Rock Mechanics and Mining Sciences*, vol. 71, pp. 340–349, 2014.

[25] S. Chen, C. Yang, and G. Wang, "Evolution of thermal damage and permeability of Beishan granite," *Applied Thermal Engineering*, vol. 110, pp. 1533–1542, 2017.

[26] W. L. Tian, S. Q. Yang, D. Elsworth, J. G. Wang, and X. Z. Li, "Permeability evolution and crack characteristics in granite under treatment at high temperature," *International Journal of Rock Mechanics and Mining Sciences*, vol. 134, article 104461, 2020.

[27] F. O. R. Triaxial, "Suggested methods for determining the strength of rock materials in triaxial compression: revised version," *International Journal of Rock Mechanics and Mining Science and Geomechanics Abstracts*, vol. 20, no. 6, pp. 285–290, 1983.

[28] W. A. M. Wanniarachchi and W. Wu, "Permeability evolution of rock-concrete interfaces in underground lined storage systems," *International Journal of Rock Mechanics and Mining Sciences*, vol. 143, article 104792, 2021.

[29] D. Zhou, Z. Zhao, B. Li, Y. Chen, and W. Ding, "Permeability evolution of grout infilled fractures subjected to triaxial compression with low confining pressure," *Tunnelling and Underground Space Technology*, vol. 104, 2020.

[30] Y. Xing, G. Zhang, T. Luo, Y. Jiang, and S. Ning, "Hydraulic fracturing in high-temperature granite characterized by acoustic emission," *Journal of Petroleum Science and Engineering*, vol. 178, pp. 475–484, 2019.

[31] Z. Yangsheng, M. Qiaorong, K. Tianhe, Z. Ning, and X. Baoping, "Micro-CT experimental technology and meso-investigation on thermal fracturing characteristics of granite," *Chinese Journal of Rock Mechanics and Engineering*, vol. 27, 2008.

[32] S. P. Clark, *Handbook of Physical Constants*, Geological Society of America, 1966.

[33] R. Tomás, M. Cano, L. F. Pulgarín et al., "Thermal effect of high temperatures on the physical and mechanical properties of a granite used in UNESCO World Heritage sites in north Portugal," *Journal of Building Engineering*, vol. 43, article 102823, 2021.

[34] T. Wang, L. Wang, F. Xue, and M. Xue, "Identification of crack development in granite under triaxial compression based on the acoustic emission signal," *International Journal of Distributed Sensor Networks*, vol. 17, no. 1, 2021.

[35] F. Kang, Y. Li, and C.'. Tang, "Grain size heterogeneity controls strengthening to weakening of granite over high-temperature treatment," *International Journal of Rock Mechanics and Mining Sciences*, vol. 145, article 104848, 2021.

[36] Q. Sun, W. Zhang, L. Xue, Z. Zhang, and T. Su, "Thermal damage pattern and thresholds of granite," *Environment and Earth Science*, vol. 74, no. 3, pp. 2341–2349, 2015.

[37] Y. Qin, H. Tian, N. X. Xu, and Y. Chen, "Physical and mechanical properties of granite after high-temperature treatment," *Rock Mechanics and Rock Engineering*, vol. 53, no. 1, pp. 305–322, 2020.

[38] X. L. Xu and M. Karakus, "A coupled thermo-mechanical damage model for granite," *International Journal of Rock Mechanics and Mining Sciences*, vol. 103, pp. 195–204, 2018.

[39] P. Jin, Y. Hu, J. Shao, G. Zhao, X. Zhu, and C. Li, "Influence of different thermal cycling treatments on the physical, mechanical and transport properties of granite," *Geothermics*, vol. 78, pp. 118–128, 2019.

[40] Y. Kang and L. You, "Effects of thermal treatment on physical property of tight rocks," *Progress in Geophysics*, vol. 24, no. 5, pp. 1850–1854, 2009.